

Clustering effects in ^{36}Ar nuclei produced via the $^{24}\text{Mg} + ^{12}\text{C}$ reaction

A. Di Nitto ^{*}, E. Vardaci , F. Davide, G. La Rana , M. Ashaduzzaman , D. Mercogliano, and P. A. Setaro 

*Dipartimento di Fisica, Università degli Studi di Napoli “Federico II”, Italy
and Istituto Nazionale di Fisica Nucleare, Sezione di Napoli, 80126 Napoli, Italy*

T. Banerjee  and A. Vanzanella

Istituto Nazionale di Fisica Nucleare, Sezione di Napoli, 80126 Napoli, Italy

D. Bianco 

Italian Aerospace Research Centre (CIRA), 81043 Capua, Italy

M. Cinausero

Laboratori Nazionali di Legnaro dell’Istituto Nazionale di Fisica Nucleare, 35020 Legnaro (Padova), Italy

N. Gelli

Istituto Nazionale di Fisica Nucleare, Sezione di Firenze, 50019 Firenze, Italy

F. Loffredo  and M. Quarto

*Advanced Biomedical Science Department, University of Naples “Federico II”, Via S. Pansini, 80131 Naples, Italy
and Istituto Nazionale di Fisica Nucleare, Sezione di Napoli, 80126 Napoli, Italy*



(Received 18 January 2023; accepted 9 February 2023; published 24 February 2023)

The nuclear properties of ^{36}Ar composite α -like nuclei produced at 46.72 MeV of excitation energy via the $^{24}\text{Mg} + ^{12}\text{C}$ reaction were investigated. In the past, at this excitation energy, resonant structures with peak-to-valley variation of 50–100 mb have been observed for this system and associated with fusion cross sections. To reveal the nature of this phenomenon the fusion channel observable was investigated. Exclusive measurements of α particles and evaporation residues were carried out at Laboratori Nazionali di Legnaro using the $8\pi\text{LP}$ apparatus coupled to an evaporation residue detector. Then the experimental data were interpreted through the comparison with statistical model predictions. The energy spectra in coincidence with evaporation residues evidence the limitation of the statistical model assuming nuclear shape of the compound nucleus according to the rotating liquid drop model. To reproduce the experimental data very elongated nuclear shapes and reduced barriers for light particle emission have to be considered, with a major to minor axis ratio up to 3 at higher angular momenta. This large value for the axis ratio is selected in agreement with the predictions of the cranked cluster model and is consistent with previous findings for α -like nuclei.

DOI: [10.1103/PhysRevC.107.024615](https://doi.org/10.1103/PhysRevC.107.024615)

I. INTRODUCTION

The clustering phenomena in light nuclei are matter of large interest [1–9]. Resonant structures peculiar of systems involving α -conjugate nuclei are the demonstration of the production and the surviving of a particular nuclear state. These resonances have been associated with α -clustering phenomena.

The harmonic oscillator has been proven to be a powerful tool in the study of nuclear clustering, as its intrinsic symmetries describe many of the features from which clustering arises. The symmetries of the deformed harmonic oscillator can be interpreted in terms of much heavier cluster components. Thus, the extent of the deformation can be described in terms of the oscillator frequencies perpendicular (ω_{\perp}) and

parallel (ω_z) to the deformation axis. Some nuclei may gain stability at certain ratios of $\omega_{\perp} : \omega_z$. These gains were observed at 2:1 and 3:1 ratios for nuclei whose proton and neutron numbers could be expressed as combinations of two and three spherical magic numbers, with configurations resembling those of molecular structures. The energy-spin plots of these states indicate large rotational momenta of inertia and, hence, large deformations. Typical examples are the so-called superdeformed and hyperdeformed rotational bands discovered for ^{40}Ca [10], and in the decay of ^{56}Ni [11], respectively.

Comparative analyses of evaporative light particle energy and angular distributions within the statistical model (SM) framework indicate nuclear deformations at high spin significantly larger than those predicted by the rotating liquid drop model (RLDM) [12]. Examples of light $N = Z$ systems showing this behavior are the ^{56}Ni [11,13], ^{48}Cr [14], ^{44}Ti [15], and ^{40}Ca [16] nuclei.

^{*}Corresponding author: adinitto@na.infn.it

Rae proposed that clustering might be an important structural feature at these shell gaps [17]. This specific feature was also reported in subsequent studies (i.e., [18]). On this basis the cranked cluster model (CCM) was developed and the calculations suggested the presence of several quasistable deformed cluster configurations at high deformations in different nuclei. According to CCM ^{36}Ar is predicted to be bound up to quite high spin ($29\hbar$) [19]. These predictions are at odds with conventional liquid drop model expectations, which suggest that ^{36}Ar nuclei should not be able to sustain such high angular momenta and excitation energies. In terms of clusters, one might describe the configurations of ^{36}Ar nuclei as $^{16}\text{O} + ^{16}\text{O} + \alpha$ [19] or $^{12}\text{C} + ^{12}\text{C} + ^{12}\text{C}$ [10] molecules. Possible relationships between quasimolecular bands and extremely deformed shapes have been widely discussed in the literature [20].

Total fusion cross section excitation function for the reaction $^{12}\text{C} + ^{24}\text{Mg}$ displays structures with peak-to-valley variation of 50–100 mb (i.e., 5–10 % of the total fusion cross section) that have been interpreted as indications of the role played by detailed properties of nuclei involved. Particularly striking is the observation that the resonance structures appearing prominently in systems involving α nuclei are relatively damped or completely absent in the neighboring systems such as the $^{12}\text{C} + ^{26}\text{Mg}$ reaction [21]. The observed gross structures show almost regular spacings of 3–5 MeV in the center of mass system and are primarily present in the channels involving the emission of α particles, which are associated with high spin states in the compound nucleus and with large partial waves in the entrance channel [21]. These behaviors, observed also in the elastic and inelastic channels are not well understood, consequently information regarding the fusion channel would be of great interest in helping to reveal the nature of these phenomena.

Correlated resonances for the $^{12}\text{C} + ^{24}\text{Mg}$ at low energies and $^{16}\text{O} + ^{20}\text{Ne}$ at higher energy reaction were observed in the elastic, inelastic, and α -transfer reactions, indicating the existence of a hyperdeformed band in ^{36}Ar [22]. The moment of inertia given by analysis is in agreement with the predictions of Rae and Merchant and the Nilsson-Strutinsky calculations [23]. The fact that similar quasimolecular states observed in the two reactions fall on the same rotational band gives further support to the interpretation of the ^{36}Ar composite system resonances.

Furthermore, the superdeformed band of ^{36}Ar was discovered in the $^{24}\text{Mg}(^{20}\text{Ne}, 2\alpha)^{36}\text{Ar}$ reaction [24] by adopting the multiple (γ -ray and charged-particle) coincidence techniques.

These considerations lead us to conclude that the structures observed in those measurements, and in particular in the fusion channel, can be investigated by measuring the particles that are evaporated at the first stages of the excited nucleus decay. Consequently, the reaction $^{24}\text{Mg} + ^{12}\text{C}$ at $E_{\text{lab}} = 91.72$ MeV producing the ^{36}Ar at the excitation energy $E_x = 46.72$ MeV was studied.

Consequently, the reaction $^{24}\text{Mg} + ^{12}\text{C}$ at $E_{\text{lab}} = 91.72$ MeV producing the ^{36}Ar at the excitation energy $E_x = 46.72$ MeV, corresponding to a resonance in the total fusion cross section observed in the by Daneshar *et al.* [21] in the inverse reaction $^{12}\text{C} + ^{24}\text{Mg}$, was studied.

The measurements were carried out at Laboratori Nazionali di Legnaro (LNL) by using the Ball of the 8π LP detector array [25] coupled to an evaporation residue detector at forward direction [26]. By exploiting the high granularity of the Ball and performing coincidence measurements with an ER selector at forward angles, we collected the α spectra over a wide angular range in order to probe the compound nucleus (CN) shape. Coincidence measurements are very effective to remove the contributions of channels not passing through the formation of CN. The beam energy is suited to populate the region in which the presence of hyperdeformations has been indicated by previous measurements and predicted by the CCM. The aim of the study is to achieve an estimate of the deformation of ^{36}Ar by adopting the procedure developed to identify the hyperdeformation as a consequence of clustering effects in ^{48}Cr nuclei [14]. In this paper we first introduce the experimental setup and the prescription adopted in the SM code LILITA_N21 [27] to simulate large deformed nuclear shapes at high angular momentum. Then we illustrate the comparison between the data and the calculations, which shows the limit of the Statistical model assuming nuclear shape of the compound nucleus according to the RLDM to reproduce exclusive observables. The improvement obtained by considering elongated nuclear shapes at high angular momenta of the emitting nucleus ^{36}Ar will be discussed in details. Complementary information about this study already appeared in [6,28].

II. EXPERIMENTAL SETUP

The experiment was performed at the tandem accelerator of Laboratori Nazionali di Legnaro (LNL). A self-supporting ^{12}C target $30\ \mu\text{g}/\text{cm}^2$ thick was bombarded with a pulsed beam of ^{24}Mg with intensity of about 8–11 nA. A beam burst had a period of 800 ns and duration of about 3 ns.

Taking into account the energy loss in the target, the beam energy of 91.72 MeV allowed to populate ^{36}Ar compound nuclei at $E_x = 46.72$ MeV in the center of target.

We used the Ball of 8π LP [25] to detect α particles, while the heavy residues were detected in an annular parallel plate avalanche counter (PPAC) placed at forward angles as shown schematically in Fig. 1. The Ball is constituted of 125 telescopes made by a first stage (ΔE) of Si detectors followed by a second stage (E) of CsI detectors, geometrically arranged with a spherical configuration. The Si detector thickness is 300 μm , mounted in the so-called flipped configuration. Each Si is followed by a 15 mm-thick CsI(Tl) crystal to stop the most energetic particles. The telescopes are distributed on seven rings placed coaxially around the beam direction at 15 cm from the target, as shown in the left panel of Fig. 1. Each ring, labeled from A to G (going from backward to forward angles) contains up to 18 telescopes pointing towards the center of the target, and covers an angular opening of about 17° . The telescopes of 1 ring at the forward direction is shown in the right panel of Fig. 1. The Ball covers the polar angle from 34° to 165° . Considering this geometry, the detectors belonging to a ring have the same average polar angle with respect to the beam axis, and all together cover the azimuthal

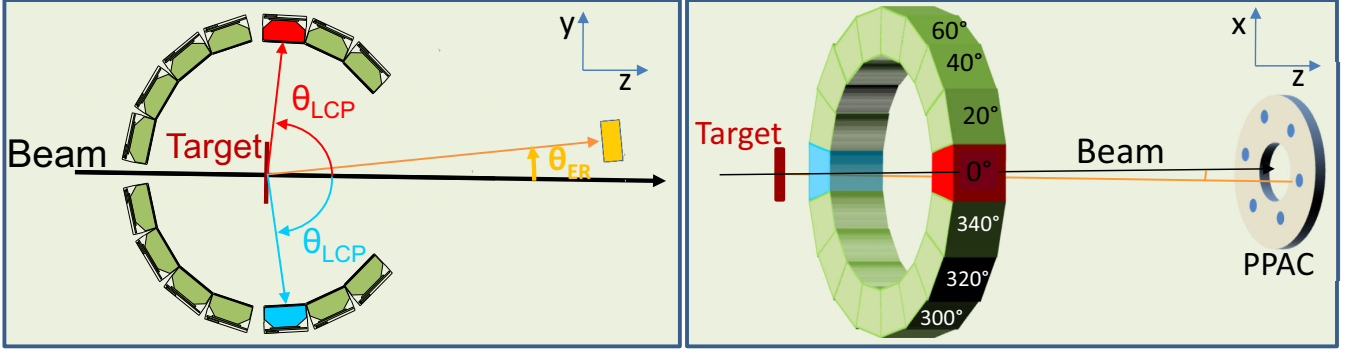


FIG. 1. Schematic layout of the experimental apparatus. On the left is shown the transversal section. The telescopes in red and blue colors belong to the same ring, i.e., they cover the same solid angle. On the right a 3D plot of the ring of the telescopes marked with blue and red. The particles collected in the red and blue detectors in coincidence with an ERs, whose mean trajectory can be described by the orange arrow ($\theta_{ER} = 4^\circ$), have the same polar angle (θ_{LCP}) and relative azimuthal angle ($\Delta\phi$) of 0° and 180° , respectively. The azimuthal angles of other detectors of the same ring with respect to the reaction plane identified by the beam and ER mean trajectory are also reported.

angle from 0° to 360° . As a whole, the Ball covers a solid angle of about 80% of 4π .

Particle identification was carried out by using the ΔE - E technique for particles having energy enough to pass through the ΔE stage, while to identify the particles that stop in the Si detectors we adopted a pulse shape discrimination technique. The combination of these two techniques allows the identification of light fragments in mass and atomic numbers as shown in [29].

The annular PPAC system, used to detect evaporation residues (ERs), is divided in six independent sectors and placed at 62 cm from the target, see Fig. 1. In order to define a narrow angular window for ERs, a mask with six holes of 1 cm diameter is mounted. Each hole subtends a solid angle of 0.8 msr and is centered at 4° with respect to the beam direction. The PPAC system consists of two coaxial PPACs (front and rear), with a propylene foil 35 μm thick mounted in between to stop the ERs passing through the front PPAC, and let the other ions, like light charged particles (LCPs) and elastically scattered beam particles, reach the rear PPAC. The ERs were therefore selected using the rear PPAC veto condition signal as anticoincidence signal for the front PPAC.

Data were collected requiring the OR mode between the following conditions: (a) events detected by any PPAC sector or by any Ball detectors to select in single mode ER and LCP events, respectively; (b) coincidences between any PPAC sector and any Ball detector to select events corresponding to the LCPs emitted in the ER channel. To reduce the system dead time only a small percentage of events in single mode have been collected, the trigger was active for one signal over 16 for the PPAC OR and one over 48 for the Ball OR. The system was set to assign a pattern for each trigger condition. However, considering the physics we are investigating, an event could have more than one pattern.

III. MODEL

In the present work, energy spectra and angular distributions are compared with the SM predictions implemented in the code LILITA_N21 [27]. The computer code LILITA_N21 is

an updated version of LILITA [30] that simulates the evaporation process taking place in the decay of excited nuclei. It models the multistep evaporative decay of a compound nucleus by using the Hauser-Feshbach formulation [31] of the SM in conjunction with the Monte Carlo method. Emissions of light particles with $Z < 3$ are taken into account, whereas fission is not considered.

The program follows the de-excitation of the CN and records in an event-by-event output file the history of each decay step. It can provide an output file by considering both the emission of a CN at rest and a CN moving in the laboratory frame. In the last decade several options were included for the transmission coefficients, the level density, and yrast lines to improve the description of the observables originating in fusion-evaporation reactions. Examples are reported in [32–38]. The prescription for the highly deformed compound nucleus shape at the high angular momentum was implemented in the code for the description of the $^{24}\text{Mg} + ^{24}\text{Mg}$ reaction [14]. Here, we performed several simulations using this prescription and more common ones. The parameters used in the simulations presented in this work are given in Table I.

The shape of a compound nucleus enters the SM through the moment of inertia and the fusion barrier of the inverse process (namely, the fusion of the residual nucleus and the

TABLE I. Input parameters for the LILITA_N21 simulations. The spherical and reduced barrier are taken from fusion systematics described in [39] and [40], respectively.

Prescription	Angular momentum		Shape	b/a at L_{max}	Barriers
	window [\hbar]				
SS	0-22		Rigid sphere	1	Spherical
RLDM	0-22		Prolate spheroid	1.32	Spherical
HD1	0-18		Rigid sphere	1	Spherical
	19-22		Prolate spheroid	3	Reduced
HD2	0-15		Rigid sphere	1	Spherical
	16-22		Prolate spheroid	2.08	Reduced

emitted particles). The moment of inertia \mathfrak{S} of a deformed nucleus is usually calculated in the SM with the following expression [41]:

$$\mathfrak{S} = \mathfrak{S}_0(1 + \delta_1 J^2 + \delta_2 J^4). \quad (1)$$

Here, the moment of inertia of a spherical nucleus, corresponding to \mathfrak{S}_0 , is modulated with the deformability parameters δ_1 and δ_2 . This ansatz scales the moment of inertia with the angular momentum J toward the one of a rigid sphere.

We performed a series of calculations whose parameters are reported in Table I. For the spherical shape (SS) we considered the nucleus as a sphere ($\delta_1 = \delta_2 = 0$) with $r_0 = 1.21$ fm and spherical transmission coefficients (TC) from fusion systematics (FS) [39] for the full range of CN angular momenta. The deformability parameters ($\delta_1 = 8 \times 10^{-5}$ and $\delta_2 = 1.77 \times 10^{-7}$) of RLDM prescription were calculated assuming an axis ratio $b/a = 1.37$ at $J = 22 \hbar$, according to the RLDM formulation in [42]. Also in the RLDM calculation spherical TC from FS were considered for the full range of angular momenta populated in the fusion reaction.

Concerning deformed calculations, two different prescriptions (HD1 and HD2) have been considered. In each calculation we defined two different windows of angular momenta. At smaller angular momenta we considered a deformability parameter of the RLDM prescription and spherical emission barriers from FS. At larger values of angular momenta we used δ_1 and δ_2 to reproduce an axis ratio up to 3 : 1 at about $J = 22 \hbar$ in combination with reduced emission barriers from systematics of Parker and collaborators [40]. The second set of parameters was introduced to describe the deviation in nuclear shapes observed in reactions with light systems at high angular momenta [14,43,44]. It is worth to remark at this point that the use of the reduced barrier is mandatory when highly deformed moments of inertia are used. More on this point will be added later on.

In order to assure a correct comparison with the experimental data, the computed observables are obtained by filtering the raw events generated by LILITA_N21 with the response function of 8π LP.

IV. RESULTS AND DISCUSSION

In this section the experimental observables collected in our experiment are presented. The comparison with the calculations suggests that the particles are emitted from a fairly deformed compound nucleus. Some further investigations based on the comparison with LILITA_N21 predictions indicate observables to be considered in future to corroborate the present conclusions.

A. Evaporation residue ToF distribution

In Fig. 2 are shown the time of flight (ToF) spectra of the particles detected by a front PPAC sector in anticoincidence with the rear PPAC (VETO condition) with different conditions. The ToF spectra were collected using a TDC in common stop mode, where the master trigger produces the start signal and the delayed radio frequency, corresponding

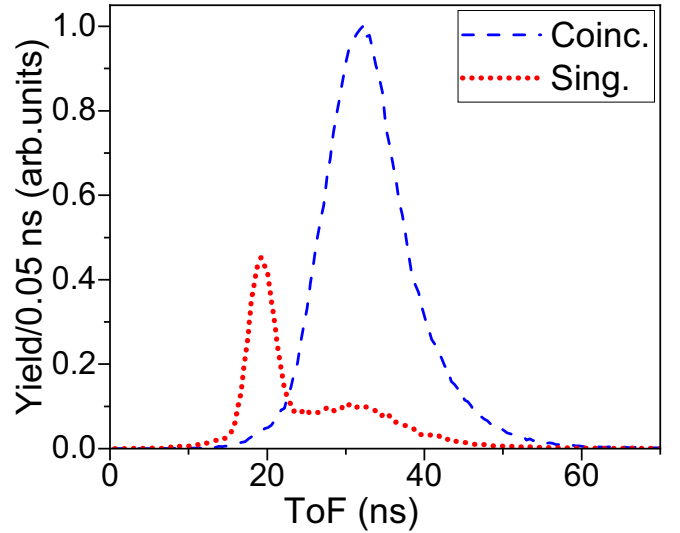


FIG. 2. Time of flight spectra of fragments detected in one PPAC sector at 4° with respect to the direction of the ^{24}Mg beam impinging on a ^{12}C target. Spectra obtained in coincidence with all Ball detector signals (dashed-blue line) and in single mode (red-dotted line). The single mode events downscaled by a factor 16 have been collected with the trigger condition b . The distributions have been normalized to the maximum of coincidence events.

to the beam pulse, the stop one. The calibration procedure and the data considered are discussed in [14]. This choice is justified by the fact that the data described in this paper were collected during the same experiment, where we benefit from the triple humped structure produced by elastic scattering and the fusion-evaporation products emerging when a ^{24}Mg beam impinges on a thin ^{24}Mg target mounted on ^{12}C backing.

The ToF spectrum measured by one of the PPAC sector in single mode (dotted-red line in Fig. 2) is still dominated by the elastic scattering (main peak on the left) because of the high counting rate of this process and the limitation in order to get the 100% efficiency with the rear PPAC. To clean the ER spectrum, the coincidence with the particles detected by the Ball has been applied (blue-dashed line in Fig. 2). Thus, the spectrum has only one peak corresponding to ERs. The same peak has been observed in the same position using the thin ^{24}Mg target mounted on ^{12}C backing [14]. This check makes us confident that the events in coincidence are in a large majority originated from the decay of ^{36}Ar compound nuclei. The absence of other peaks indicates a negligible contribution of different reactions. α particles in the ER channel were measured as coincidence events according to the trigger condition b and a ToF larger than 30 ns. The probability to collect particles from other processes is made negligible by the following conditions: the use of a self-supporting target; the low probability of random coincidences between particles in the Ball detectors; the reduced elastic-scattering rate achieved by introducing both the VETO conditions, the few hundred nanosecond gate for coincidence, and the selection of ToF range.

The count integral associated to the elastic scattering and to the ERs in all the PPAC sectors placed in the six corners of

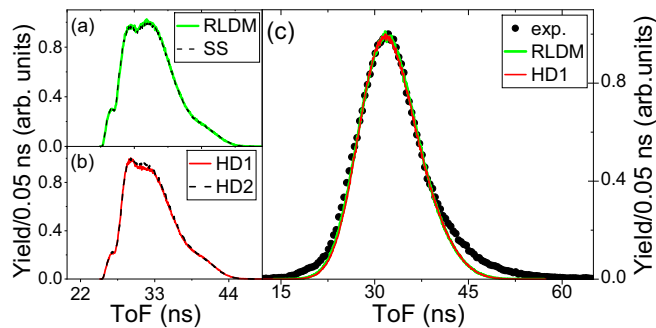


FIG. 3. Evaporation-residue time of flight spectra at 4° in coincidence with charged particles. On the left are shown the computed spectra without including the detector time resolution. The coincidence in calculations consists of at least a charged particle emitted in the angular range $\theta_{\text{lab}} = 34\text{--}164^\circ$. In (a) and (b) are compared the spectra obtained with the prescriptions SS and RLDM, and HD1 and HD2, respectively. In (c) the RLDM and HD1 spectra, including the spread due to the time resolution, are superimposed to the experimental spectrum. The experimental spectrum is collected with the trigger- b condition, i.e., nonvetoed ToF in coincidence with $8\pi\text{LP}$ Ball telescope signals. All the spectra are normalized to the maximum. For more details see the text.

a regular hexagon centered in the beam was fairly constant. Therefore, we have considered the beam impinging on the target well aligned. All the summing procedures considering the same angular correlations between ER and particles to extract the evaporation-channel observables are doable without corrections.

The ToF spectra obtained by considering the fusion-evaporation residues were computed by LILITA_N21 and filtered by the apparatus response function. The response function considers the angular range of the $8\pi\text{LP}$ Ball detectors ($\theta_{\text{lab}} = 34\text{--}164^\circ$) for the light particle and the angular range of the PPAC sector opening angle ($\theta_{\text{lab}} = 3.5\text{--}4.5^\circ$). Furthermore, an experimental time resolution, computed assuming a Gaussian with a standard deviation $\sigma t = 3$ ns to take into account the PPAC time performances as well as the beam burst length of 3 ns, was considered. The differences between the calculations assuming a spherical or almost spherical emitters (SS and RLDM) are negligible, see Fig. 3(a). Similar situations are observed also for the calculations in which emitters with prolate shapes are considered (HD1 and HD2), see Fig. 3(b).

Once also the experimental time resolution is taken into account, the ToF spectra of all calculations well reproduce the experimental distribution, see Fig. 3(c). This observation from one side confirms the thesis of a negligible amount of polluting processes, and from the other allows to determine the percentage of ER in different time intervals with respect to the total. Consequently, the simulation helped us to estimate the total ER events in single mode within a time interval (ToF > 30 ns) that allows to minimize the contribution of elastic scattering. This correction factor is evaluated by considering the total ER-LCP coincidence and those occurring in the time interval used to select the ERs in the single mode. The total amount of ER-LCP coincidences in the time window is

$90 \pm 3\%$. The uncertainty is estimated to include all the values obtained from the different PPAC sectors.

Unfortunately, by including the experimental time resolution all the differences existing between the deformed and spherical calculations disappear. Therefore, the ToF spectrum, collected with the sensitivity reached in these experimental conditions, is not sensitive enough to shed light on the most appropriate model to describe the shape assumed by the emitting nuclei.

B. α particle energy spectra

In order to characterize the decay of compound nuclei, α -particle energy spectra measured at different angles have been compared with calculations. By taking into account the changes in energy spectra as function in the laboratory system and the response function of the apparatus, in the α particle spectra measured in coincidence with the evaporation residues the contributions from nonequilibrated sources, i.e., different from the compound nucleus, are negligible. In Fig. 4 selected calculations, whose parameters are given in Table I, are superimposed to three samples of experimental spectra. The three spectra are collected considering different telescopes of $8\pi\text{LP}$ and PPAC sectors. The differences among energy spectra calculated with the two almost spherical prescriptions (SS and RLDM), independently on the angle considered, are negligible and can be considered merely statical fluctuations. This occurs because, being involved in the decay cascades only very light nuclei, the deformations predicted by the RLDM remain quite low and gradually decrease along the decay cascades. At the largest angular momenta of compound nuclei, $22\hbar$, the axis ratio b/a is equal to 1.32 according to the RLDM [42]. Neither of these two calculations assuming spherical shapes, or close to spherical, reproduce the experimental data. Whereas by introducing a notable amount of deformations, as adopting the HD1 and HD2, where an axis ratio b/a of 3 and 2.08 is reached, respectively, the experimental spectra are much better reproduced.

Usually the evaporative spectra at high energy side show a single slope. This is due to the facts that the energy spectra are produced by the convolution of particles from different evaporative cascades and by considering a detector opening wide enough to include particles that when emitted at different angles have different energies. Although double bumps for this type of reaction are not usually evidenced in measurements, they are very useful because they allow to partially disentangle the different components of the spectra. In this study we observed that a double bump structure becomes visible in the spectra collected with the detectors at $\theta_{\text{lab}} = 78^\circ$ and $\theta_{\text{lab}} = 61^\circ$ (Fig. 4). In the spectrum at $\theta_{\text{lab}} = 78^\circ$ we can see two bumps. The first is at around 8 MeV, relatively close to the maximum of the spectrum, and the second, which is more separated from the maximum, at around 16 MeV. This latter bump is still visible in detectors at $\theta_{\text{lab}} = 61^\circ$, however, in this more forward direction, the energy corresponding to the center of the bump is larger and it is at around 20 MeV. These bumps are not accidental, but are related to specific decay channels, whose contribution is enhanced by the

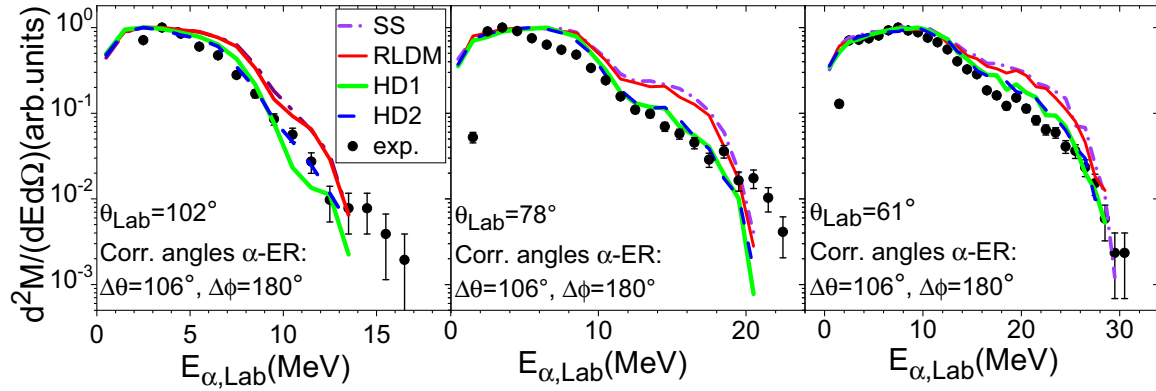


FIG. 4. α -particle energy spectra measured in coincidence with ERs detected at forward direction at three different laboratory angles. The experimental data (dots) are compared with the predictions of the statistical model prescriptions: SS (dash-dotted violet line), RLDM (solid red line), the HD1 (solid green line), and HD2 (dashed blue line). The prescription parameters are given in Table I. Between the experimental energy spectra there is not a single detector element in common, both telescopes of the 8π LP Ball and PPAC sectors considered are different. See the text for details.

peculiar angular correlation between the light particles and the evaporation residues considered.

To better understand this aspect and the potentiality to get more insight on the evolution of nuclear shape in light nuclei as function of the angular momentum, a detailed comparison between LLLITA_N21 predictions has been performed. The two most representative calculations, the one assuming the SS and the one including the largest deformations (HD1), are presented in Fig. 5, for the 2α and $1p1\alpha$ channels, as an example.

The calculation results show that the increase of nuclear deformations occurring at high angular momenta slightly modifies the kinetic energy of α particles in the specific channels, whereas it also strongly affects the competition among the exit channels. This competition can be investigated because it modulates the shapes of the evaporative spectra. The reduction of the bump at around 16 MeV, discussed above, is

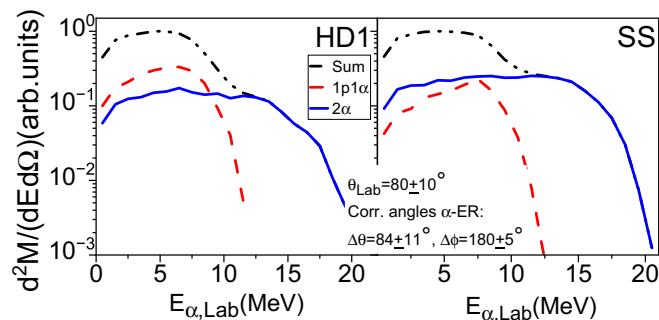


FIG. 5. Calculated α -particle energy spectra in coincidence with ERs. The simulations are filtered considering an α particle emitted at $\theta_{lab} = 80^\circ$ in coincidence with ERs at $\theta_{lab} = 4^\circ$. The two particles are emitted in the same plane but the opposite sides with respect to beam direction $\Delta\phi = 180^\circ$. The statistical model calculations using the HD1 (left panel) and SS (right panel) prescriptions are presented. The spectrum including all α channels (dashed-dotted-dotted black line) and the two most probable exit channels (2α solid blue line and $1p1\alpha$ dashed red line) are reported. See the text for details.

due to the decrease of the probability of the 2α decay channel with respect to the others. This 2α decrease occurs because of the lowering of the yrast line due to the larger moment of inertia of deformed nuclei. Therefore, it favors the emission at the first step of the decay cascades of protons removing a smaller amount of angular momentum with respect to the α particles. Thus, from the reduced 2α and the increased $1p1\alpha$ channel probabilities result in a softer α particle energy spectrum, see Fig. 5. The effects on the other channels involving at least one α particle are instead much smaller, indicating emission from compound nuclei of smaller angular momenta. The less pronounced bumps, observed in the HD1 and HD2 calculations and in the experimental data, indicate the α -particle emission from elongated nuclei.

For these reasons it would be very elucidating to investigate in details all the channels involving at least two light charged particles in terms of angular correlations and multiplicities. Unfortunately, the statistics collected in this experiment was insufficient to extract a series of more exclusive observables as it was done for instance in [14].

C. Proton energy spectra

The compound nucleus deformation gives rise to a distribution of Coulomb barriers between the particle and the residual nucleus. This distribution extends down to energies lower than the spherical barrier and thus enhances the probability to evaporate low-energy particles. Therefore, by increasing nuclear deformations more soft particle energy spectra are expected, see for instance [44,45].

Accordingly, one can expect that the nuclear deformation will also affect proton energy spectra. In many studies, as for instance [14,46,47], the proton spectra have not been considered, as their energy spectra have shown less sensitivity to the nuclear deformation. This behavior is confirmed if we consider our calculated proton spectra at $\theta_{lab} \leq 80^\circ$ and $\theta_{lab} \geq 140^\circ$ both in coincidences with ERs at 4° : the differences between the four prescriptions are negligible, as shown in Fig. 6(a) and 6(d). However, by considering some specific

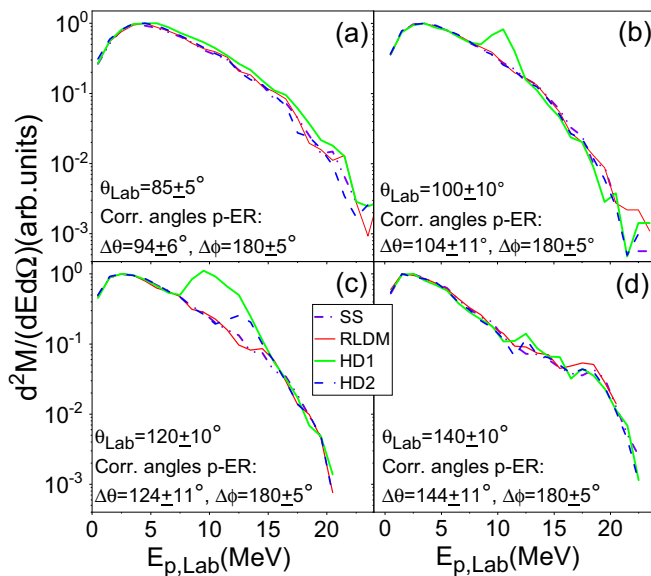


FIG. 6. Calculated proton energy spectra in coincidence with ERs. The events are generated in the laboratory frame and then filtered by considering protons emitted at different angles always in coincidence with ERs emitted at 4° . The two particles are emitted in the same plane, but on opposite sides with respect to the beam direction ($\Delta\phi = 180^\circ$).

angular correlations between protons and ERs the differences in the energy spectra calculated by assuming spherical and deformed emitters can be notable. In Fig. 6(c) and 6(d) a bump with a maximum at 9.5 MeV is predicted for the two HD prescriptions. At a first glance, the presence of the proton bump seems to compensate for the decrease of those featuring the α -particle spectra, discussed above.

A more in-depth analysis aimed at identifying the channel determining the origin of the bump was performed by considering only the two prescriptions with the largest difference in terms of deformations, i.e., the SS and HD1. The energy distributions produced by all exit channels in which there is the emission of at least one proton have been disentangled from the the proton spectra. In Fig. 7 a large bump in the the energy spectrum at $\theta_{\text{lab}} = 120^\circ \pm 10^\circ$ is observed when the HD1 is considered, whereas in the same energy region a smooth slope at the high-energy side is predicted by calculations with the SS prescription. Looking at the contributions of different channels it is clear that the high-energy protons are produced solely from those involving up to two particles. In these conditions, indeed, a large amount of available energy is removed by a single proton and the resulting decay cascades are shorter.

Furthermore, different from what happens for the α particles, by using different prescriptions there is a change not only in the exit channel probabilities, but also in the energy distributions of a specific channel, as one can infer from Figs. 5 and 7. We can see in Fig. 7 how well pronounced the changes are that occur in the $1p$ channel. Here, the peak in the HD1 calculations is almost two orders of magnitude more intense and its maximum, at about 10 MeV, is shifted at lower energy compared to the SS calculations. The explanation of

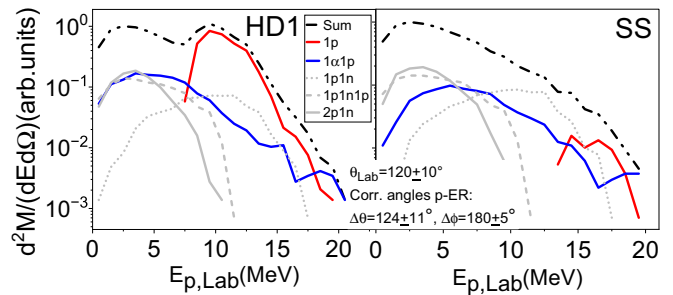


FIG. 7. Calculated proton energy spectra in coincidence with ERs. The simulations are filtered considering proton emitted at $\theta_{\text{lab}} = 120^\circ$ in coincidence with ERs at $\theta_{\text{lab}} = 4^\circ$. The particle and ER are emitted in the same plane, but the opposite sides with respect to beam direction ($\Delta\phi = 180^\circ$). The statistical model calculations using the HD1 (left panel) and SS (right panel) prescriptions are presented. In each panel are reported the spectrum including all protons channels (dashed-dotted-dotted black line), two exit channels whose probabilities increases by including deformations ($1p1\alpha$ solid-blue line and $1p$ solid-red line), and several exit channels with a high probability independent on deformation ($2p1n$ solid-gray line, $1p1n$ dashed-gray line, and $1p1n1p$ dotted-gray line). See the text for more details.

a such behavior is related to the nuclear shapes involved. Indeed, the energy available for the particle emission in the yrast plane depends on the shape of the yrast line. At higher angular momenta the rotational energy corresponding to the SS yrast line is so high that the probability of proton emission at the first step becomes negligible, whereas by introducing a deformation at the higher spin the reduction of the rotational energy makes it more probable. Although with HD1 prescription the energy available increases, it remains quite low, therefore the emission of low-energy protons generating excited nuclei in the neighboring of the yrast line largely increases. In the long decay cascades the recoil effect on the residual nuclei due to the light-particle emission is smeared out at each decay step. In the short cascades this is not the case and a strong kinematic correlation is established between proton and evaporation residue trajectories. Consequently, when the evaporation residues emitted at around $\theta_{\text{lab}} = 4^\circ$ are considered, the contribution of the $1p$ channel is very pronounced only in an angular interval at around 120° , as shown in Fig. 7.

At the same time the increase of the $1p$ channel yield at high angular momenta significantly reduces the probability of the emission of particles removing large angular momenta, explaining the observed reduction of the 2α channel discussed in Sec. IV B.

V. SUMMARY AND CONCLUSIONS

α particles emitted in the $^{24}\text{Mg} + ^{12}\text{C}$ reaction at $E_{\text{lab}} = 91.72$ MeV have been measured in coincidence with ERs using the 8π LP apparatus at LNL. The statistical model analysis, taking into account the response function of the apparatus, indicates that the α particles are emitted predominantly from equilibrated compound nuclear sources.

We found that a significant amount of deformation at high angular momenta, much larger than the one predicted by

the RLDM, is needed in the model to explain the measured spectra satisfactorily. In particular statistical model calculations have been carried out assuming: (i) spherical moment of inertia and TC from fusion systematics [39]; (ii) deformed moment of inertia with spin-dependent deformation parameters (δ_1 and δ_2) and TC according the systematics for deformed nuclei of [48] at high angular momenta, and deformability parameter of RLDM prescription and spherical emission barriers from FS at smaller angular momenta. Effective deformability parameters extracted with option ii) are in agreement with those obtained for the α -like $^{24}\text{Mg} + ^{24}\text{Mg}$ system, indicating large overall deformations with an axis ratio up to 3 : 1 (hyperdeformed configuration) at higher angular momentum. The axis ratio value has been selected in agreement with the predictions of the cranked cluster model calculations in [19] which reproduces, for the $^{24}\text{Mg} + ^{24}\text{Mg}$ reaction, the resonant decay flux in the inelastic and elastic channels [49] and, assumed in the SM calculations, the energy spectra, the multiplicity, the double, and the triple correlations of α particles [14]. This may be another signature of the formation of a long-lived orbiting-like dinuclear system at high excitation energies (40–60 MeV) from light-particle emission studies of α -like nuclei.

Although the α spectra in correlations with evaporation residues measured at different angles suggest the existence of large deformations, for a conclusive indication additional probes need to be considered. This motivates further simulations. The cluster model predicts the surviving of largely deformed nuclei at high angular momenta, consequently, due

to the reduction of the yrast line, the probability to populate the $1p$ channel is increased. We have shown that such an increase can be effectively evidenced, because the mean energy of protons emitted in short decay cascades is larger than that of protons of long decay cascades. In particular, the simulations with the ii) option predict a large bump in the energy spectra in coincidence with evaporation residues emitted at specific angles, which are due to the $1p$ channel and represents the solid experimental signature we searched for. This comprehensive study evidenced once more the importance to collect a large data set of very exclusive observables to probe the properties of excited nuclei and, in particular, the evolution of the nuclear shape as function of the angular momenta. In conclusion, the comparison of our measurements with the predictions of the SM for the $^{24}\text{Mg} + ^{12}\text{C}$ reaction indicates the formation of hyperdeformed configurations in compound nuclei whose properties can be probed by studying the evaporation channels. The occurrence of these shapes is predicted by the cranked cluster model and confirms the peculiar nature of the $N = Z$ nuclei. These nuclei, differently from the neighboring, can survive even at high angular momenta by rearranging the α -particle constituents by assuming extremely elongated shapes far beyond the expectations of the rotating liquid drop model.

ACKNOWLEDGMENT

The authors wish to thank the staff at LNL for the excellent support in carrying out this experiment.

-
- [1] H. Horiuchi, Y. Kanada-En'yo, and M. Kimura, *Nucl. Phys. A* **722**, C80 (2003).
- [2] H. Horiuchi, *Nucl. Phys. A* **731**, 329 (2004).
- [3] H. Horiuchi, *Clusters in Nuclei*, Lecture Notes in Physics, Vol. 818 (Springer, Berlin, 2010), p. 57.
- [4] S. Thummerer, W. von Oertzen, B. Gebauer, S. M. Lenzi, A. Gadea, D. R. Napoli, C. Beck, and M. Rousseau, *J. Phys. G: Nucl. Part. Phys.* **27**, 1405 (2001).
- [5] W. von Oertzen, *Clusters in Nuclei*, Lecture Notes in Physics, Vol. 818 (Springer, Berlin, 2010), p. 109.
- [6] E. Vardaci, A. Di Nitto, P. Nadochty, A. Brondi, G. La Rana, R. Moro, A. Vanzanella, M. Cinausero, G. Prete, and N. Gelli, *J. Phys.: Conf. Ser.* **436**, 012054 (2013).
- [7] C. Beck and A. Szanto de Toledo, *Phys. Rev. C* **53**, 1989 (1996).
- [8] C. Beck, *J. Phys.: Conf. Ser.* **863**, 012002 (2017).
- [9] N. Alamanos, C. Bertulani, and V. Guimarães, *Eur. Phys. J. A* **57**, 196 (2021).
- [10] S. M. Singer, W. N. Catford, G. J. Gyapong, M. Shawcross, N. M. Clarke, N. Curtis, M. Freer, B. R. Fulton, S. J. Hall, R. A. Le Marechal, M. J. Leddy, J. S. Pople, G. Tungate, R. P. Ward, W. D. M. Rae, P. M. Simmons, S. P. G. Chappell, S. P. Fox, C. D. Jones, P. Lee, and D. L. Watson, *Phys. Rev. C* **62**, 054609 (2000).
- [11] W. von Oertzen, B. Gebauer, G. Efimov, V. Zhrebchevsky, Tz. Kokalova, S. Thummerer, Ch. Schulz, H. G. Bohlen, D. Kamanin, C. Beck, D. Curien, P. Papka, M. Rousseau, G. Royer, and G. de Angelis, *Eur. Phys. J. A* **36**, 279 (2008).
- [12] A. J. Sierk, *Phys. Rev. C* **33**, 2039 (1986).
- [13] C. Bhattacharya, M. Rousseau, C. Beck, V. Rauch, R. M. Freeman, D. Mahboub, R. Nouicer, P. Papka, O. Stezowski, A. Hachem, E. Martin, A. K. Dummer, S. J. Sanders, and A. Szanto De Toledo, *Phys. Rev. C* **65**, 014611 (2001).
- [14] A. Di Nitto, E. Vardaci, A. Brondi, G. La Rana, M. Cinausero, N. Gelli, R. Moro, P. N. Nadochty, G. Prete, and A. Vanzanella, *Phys. Rev. C* **93**, 044602 (2016).
- [15] P. Papka, C. Beck, F. Haas, V. Rauch, M. Rousseau, P. Bednarczyk, S. Courtin, O. Dorvaux, K. Eddahbi, J. Robin, A. Sánchez i Zafra, O. Stezowski, and A. Prévost, *Acta Phys. Pol. B* **34**, 2343 (2003).
- [16] M. Rousseau, C. Beck, C. Bhattacharya, V. Rauch, O. Dorvaux, K. Eddahbi, C. Enaux, R. M. Freeman, F. Haas, D. Mahboub, R. Nouicer, P. Papka, O. Stezowski, S. Szilner, A. Hachem, E. Martin, S. J. Sanders, A. K. Dummer, and A. Szanto de Toledo, *Phys. Rev. C* **66**, 034612 (2002).
- [17] W. D. M. Rae, *Int. J. Mod. Phys. A* **03**, 1343 (1988).
- [18] W. Nazarewicz and J. Dobaczewski, *Phys. Rev. Lett.* **68**, 154 (1992).
- [19] W. D. M. Rae and A. C. Merchant, *Phys. Lett. B* **279**, 207 (1992).
- [20] C. Beck, P. Papka, A. Sánchez i Zafra, S. Thummerer, F. Azaiez, P. Bednarczyk, S. Courtin, D. Curien, O. Dorvaux, D. Lehbertz, A. Nourredine, M. Rousseau, W. von Oertzen, B. Gebauer, C. Wheldon, Tz. Kokalova, G. de Angelis, A. Gadea, S. Lenzi, S.

- Szilner, D. R Napoli, W. N. Catford, D. G. Jenkins *et al.*, *Phys. Rev. C* **80**, 034604 (2009).
- [21] K. Daneshvar, D. G. Kovar, S. J. Krieger, and K. T. R. Davies, *Phys. Rev. C* **25**, 1342 (1982).
- [22] A. Lépine-Szily, W. Sciani, E. A. Benjamim, L. C. Chamon, R. Lichtenthäler, and Y. Otani, *J. Phys.: Conf. Ser.* **111**, 012037 (2008).
- [23] J. Cseh, J. Darai, W. Sciani, Y. Otani, A. Lépine-Szily, E. A. Benjamim, L. C. Chamon, and R. Lichtenthäler Filho, *Phys. Rev. C* **80**, 034320 (2009).
- [24] C. E. Svensson, E. Caurier, A. O. Macchiavelli, A. Juodagalvis, A. Poves, I. Ragnarsson, S. Åberg, D. E. Appelbe, R. A. E. Austin, C. Baktash, G. C. Ball, M. P. Carpenter, E. Caurier, R. M. Clark, M. Cromaz, M. A. Deleplanque, R. M. Diamond, P. Fallon, M. Furlotti, A. Galindo-Uribarri, R. V. F. Janssens *et al.*, *Phys. Rev. Lett.* **85**, 2693 (2000).
- [25] E. Fioretto, M. Cinausero, M. Giacchini, M. Lollo, G. Prete, R. Burch, M. Caldogno, D. Fabris, M. Lunardon, G. Nebbia, G. Viesti, A. Boiano, A. Brondi, G. La Rana, R. Moro, A. Ordine, E. Vardaci, A. Zoghi, N. Gelli, and F. Lucarelli, *IEEE Trans. Nucl. Sci.* **44**, 1017 (1997).
- [26] A. Di Nitto, E. Vardaci, G. La Rana, P. N. Nadtochy, and G. Prete, *Nucl. Phys. A* **971**, 21 (2018).
- [27] F. Davide, A. Di Nitto, E. Vardaci, and G. La Rana, *Nucl. Instrum. Methods Phys. Res. A* **1025**, 166178 (2022).
- [28] A. Di Nitto, A. Brondi, G. La Rana, R. Moro, P. Nadtochy, E. Vardaci, A. Vanzanella, M. Cinausero, G. Prete, and N. Gelli, *EPJ Web Conf.* **21**, 02002 (2012).
- [29] E. Vardaci, P. K. Rath, M. Mazzocco, A. Di Nitto, G. La Rana, C. Parascandolo, D. Pierrousakou, M. Romoli, A. Boiano, A. Vanzanella, M. Cinausero, G. Prete, N. Gelli, F. Lucarelli, C. Mazzocchi, M. La Commara, L. Fortunato, A. Guglielmetti, F. Soramel L. Stroe, and C. Signorini, *Eur. Phys. J. A* **57**, 95 (2021).
- [30] J. Gomez del Campo and R. G. Stokstad, Oak Ridge National Laboratory Report No. TM7295, 1981.
- [31] W. Hauser and H. Feshbach, *Phys. Rev.* **87**, 366 (1952).
- [32] A. Di Nitto, E. Vardaci, A. Brondi, G. La Rana, R. Moro, P. N. Nadtochy, M. Trotta, A. Ordine, A. Boiano, M. Cinausero, E. Fioretto, G. Prete, V. Rizzi, D. V. Shetty, M. Barbui, D. Fabris, M. Lunardon, G. Montagnoli, S. Moretto, G. Viesti, N. Gelli, F. Lucarelli *et al.*, *Eur. Phys. J. A* **47**, 83 (2011).
- [33] R. Moro, A. Brondi, N. Gelli, M. Barbui, A. Boiano, M. Cinausero, A. Di Nitto, D. Fabris, E. Fioretto, G. La Rana, F. Lucarelli, M. Lunardon, G. Montagnoli, A. Ordine, G. Prete, V. Rizzi, M. Trotta, and E. Vardaci, *Eur. Phys. J. A* **48**, 159 (2012).
- [34] E. Vardaci, P. N. Nadtochy, A. Di Nitto, A. Brondi, G. La Rana, R. Moro, P. K. Rath, M. Ashaduzzaman, E. M. Kozulin, G. N. Knyazheva, I. M. Itkis, M. Cinausero, G. Prete, D. Fabris, G. Montagnoli, and N. Gelli, *Phys. Rev. C* **92**, 034610 (2015).
- [35] T. Hüyük, A. Di Nitto, G. Jaworski, A. Gadea, J. J. Valiente-Dobón, J. Nyberg, M. Palacz, P.-A. Söderström, R. J. Aliaga-Varea, G. de Angelis, A. Ataç, J. Collado, C. Domingo-Pardo, F. J. Egea, N. Erduran, S. Ertürk, G. de France, R. Gadea, V. González, V. Herrero-Bosch *et al.*, *Eur. Phys. J. A* **52**, 55 (2016).
- [36] E. Vardaci, A. Di Nitto, P. N. Nadtochy, and G. La Rana, *J. Phys. G: Nucl. Part. Phys.* **46**, 115111 (2019).
- [37] A. Di Nitto, E. Vardaci, G. La Rana, P. N. Nadtochy, A. Boiano, M. Cinausero, G. Prete, N. Gelli, E. M. Kozulin, G. N. Knyazheva, A. Ordine, F. Davide, C. Parascandolo, D. Pierrousakou, and A. Pulcini, *Phys. Rev. C* **102**, 024624 (2020).
- [38] A. Di Nitto, F. Davide, E. Vardaci, D. Bianco, G. La Rana, and D. Mercogliano, *Appl. Sci.* **12**, 4107 (2022).
- [39] L. C. Vaz and J. M. Alexander, *Z. Phys. A* **318**, 231 (1984).
- [40] W. E. Parker, M. Kaplan, D. J. Moses, G. La Rana, D. Logan, R. Lacey, J. M. Alexander, D. M. de Castro Rizzo, P. De Young, R. J. Welberry, and J. T. Boger, *Phys. Rev. C* **44**, 774 (1991).
- [41] J. R. Huizenga, A. N. Behkami, I. M. Govil, W. U. Schröder, and J. Töke, *Phys. Rev. C* **40**, 668 (1989).
- [42] S. Cohen, F. Plasil, and W. J. Swiatecki, *Ann. Phys. (NY)* **82**, 557 (1974).
- [43] C. M. Brown, Z. Milosevich, M. Kaplan, E. Vardaci, P. DeYoung, J. P. Whitfield, D. Peterson, C. Dykstra, P. J. Karol, and M. A. McMahan, *Phys. Rev. C* **60**, 064612 (1999).
- [44] G. La Rana, D. J. Moses, W. E. Parker, M. Kaplan, D. Logan, R. Lacey, J. M. Alexander, and R. J. Welberry, *Phys. Rev. C* **35**, 373 (1987).
- [45] R. J. Charity, L. G. Sobotka, J. Cibor, K. Hagel, M. Murray, J. B. Natowitz, R. Wada, Y. El Masri, D. Fabris, G. Nebbia, G. Viesti, M. Cinausero, E. Fioretto, G. Prete, A. Wagner, and H. Xu, *Phys. Rev. C* **63**, 024611 (2001).
- [46] G. La Rana, R. Moro, A. Brondi, P. Cuzzocrea, A. D'Onofrio, E. Perillo, M. Romano, F. Terrasi, E. Vardaci, and H. Dumont, *Phys. Rev. C* **37**, 1920 (1988).
- [47] A. Dey, S. Bhattacharya, C. Bhattacharya, K. Banerjee, T. K. Rana, S. Kundu, S. Mukhopadhyay, D. Gupta, and R. Saha, *Phys. Rev. C* **74**, 044605 (2006).
- [48] W. E. Parker, M. Kaplan, D. J. Moses, J. M. Alexander, J. T. Boger, R. A. Lacey, and D. M. de Castro Rizzo, *Nucl. Phys. A* **568**, 633 (1994).
- [49] A. H. Wuosmaa, R. W. Zurmühle, P. H. Kutt, S. F. Pate, S. Saini, M. L. Halbert, and D. C. Hensley, *Phys. Rev. C* **41**, 2666 (1990).